AGU PUBLICATIONS

JGR

Journal of Geophysical Research: Solid Earth

RESEARCH ARTICLE
10.1002/2016JB013467

Key Points:
- The Newport-Inglewood/Rose Canyon fault zone appears to be one, continuous fault zone, with small stepovers
- This study finds four main strands and three main stepovers in the NIRC fault zone
- Ruptures on this fault could produce up to *M* 7.4 earthquake

Supporting Information:
- Supporting Information S1

Correspondence to:
V. Sahakian,
vsahakian@usgs.gov

Citation:
Sahakian, V., J. Bormann, N. Driscoll, A. Harding, G. Kent, and S. Wesnousky (2017), Seismic constraints on the architecture of the Newport-Inglewood/Rose Canyon fault: Implications for the length and magnitude of future earthquake ruptures, *J. Geophys. Res. Solid Earth*, *122*, 2085–2105, doi:10.1002/2016JB013467.

Received 16 AUG 2016
Accepted 6 FEB 2017
Accepted article online 7 MAR 2017
Published online 11 MAR 2017

Seismic constraints on the architecture of the Newport-Inglewood/Rose Canyon fault: Implications for the length and magnitude of future earthquake ruptures

Valerie Sahakian[1,2], Jayne Bormann[3,4], Neal Driscoll[1], Alistair Harding[1], Graham Kent[2], and Steve Wesnousky[2]

[1]Scripps Institution of Oceanography, University of California, San Diego, La Jolla, California, USA, [2]Now at Earthquake Science Center, U.S. Geological Survey, Menlo Park, California, USA, [3]Nevada Seismological Laboratory, University of Nevada, Reno, Reno, Nevada, USA, [4]Now at Department of Geological Sciences, California State University, Long Beach, Long Beach, CA, USA

Abstract The Newport-Inglewood/Rose Canyon (NIRC) fault zone is an active strike-slip fault system within the Pacific-North American plate boundary in Southern California, located in close proximity to populated regions of San Diego, Orange, and Los Angeles counties. Prior to this study, the NIRC fault zone's continuity and geometry were not well constrained. Nested marine seismic reflection data with different vertical resolutions are employed to characterize the offshore fault architecture. Four main fault strands are identified offshore, separated by three main stepovers along strike, all of which are 2 km or less in width. Empirical studies of historical ruptures worldwide show that earthquakes have ruptured through stepovers with this offset. Models of Coulomb stress change along the fault zone are presented to examine the potential extent of future earthquake ruptures on the fault zone, which appear to be dependent on the location of rupture initiation and fault geometry at the stepovers. These modeling results show that the southernmost stepover between the La Jolla and Torrey Pines fault strands may act as an inhibitor to throughgoing rupture due to the stepover width and change in fault geometry across the stepover; however, these results still suggest that rupture along the entire fault zone is possible.

1. Introduction

The Newport-Inglewood/Rose Canyon (NIRC) fault zone poses a significant hazard to coastal Southern California because of its close proximity to some of the most densely populated regions of North America, such as San Diego, Orange, and Los Angeles counties as well as Tijuana, Mexico. This fault zone is the easternmost of the offshore Inner Continental Borderlands (ICB) fault system, and it is an active component of the Pacific-North America plate boundary (Figure 1). Modern plate boundary deformation in the ICB is accommodated primarily on high-angle strike-slip faults, with localized regions of transpression and transtension resulting from geometrical complexities along the faults [e.g., *Ryan et al.*, 2009; *Maloney et al.*, 2016]. Together, faults between the shoreline and San Clemente Island accommodate approximately 5–8 mm/yr of Pacific-North American plate boundary motion [*Bennett et al.*, 1996]. Between 0.5 and 2 mm/yr of this motion is partitioned on the NIRC fault zone [*Freeman et al.*, 1992; *Lindvall and Rockwell*, 1995]. Fault geometry plays a controlling role in limiting the extent of earthquake ruptures [e.g., *Sibson*, 1985; *King and Nabelek*, 1985; *Wesnousky*, 2006]. Newly acquired high-resolution seismic data and reprocessed legacy industry seismic data are employed here to improve the characterization of geometry and segmentation of the offshore NIRC fault zone, between La Jolla and Newport Beach (Figure 1). This study seeks to understand potential rupture lengths and magnitudes of earthquake ruptures on the offshore segments of the NIRC fault. The increased resolution of mapping refines the fault geometry and contributes to the improvement of seismic hazard models for the adjacent coast.

2. Background: Prior Fault and Earthquake Studies

Onshore the NIRC fault zone strikes northward from San Diego Bay to La Jolla, where it uplifts Mount Soledad as the result of a left jog, before stepping offshore, south of La Jolla Canyon (Figure 1). The fault extends to the

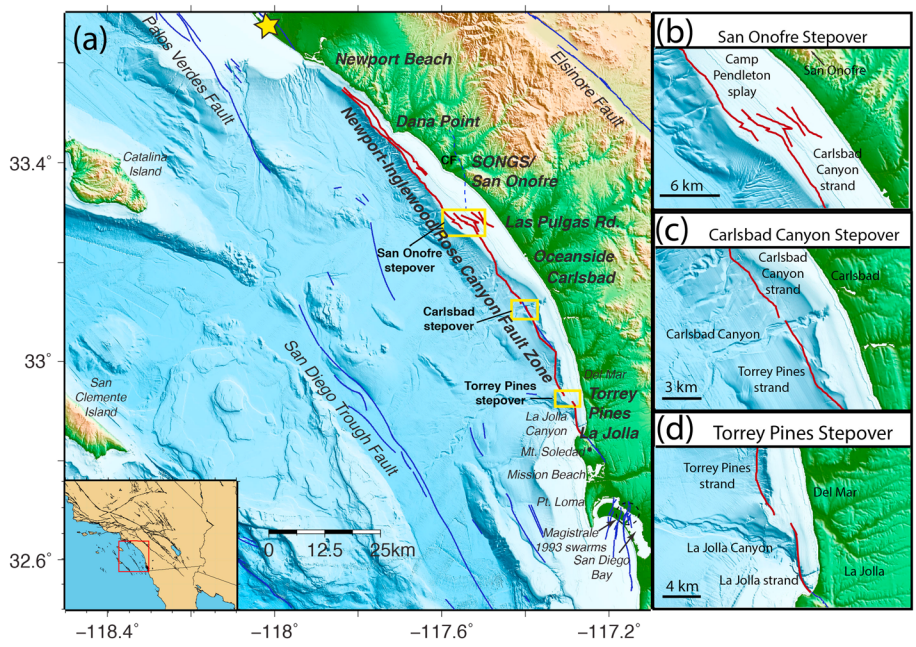

Figure 1. (a) Regional fault map. The red box in the inset shows the location of this regional map. Faults and landmarks mentioned in this paper are denoted on the map. The blue lines are the Holocene to latest Pleistocene faults from the USGS Quaternary Fault and Fold Database [*U.S. Geological Survey and California Geological Survey*, 2006], and the red lines are the mapped Newport-Inglewood/Rose Canyon fault zone based on new and reprocessed nested geophysical data. The dashed blue line is the Cristianitos Fault (CF) as shown in *Klotsko et al.* [2015]. The yellow boxes indicate the locations of the three stepovers identified in this study. The thin dashed circle shows the approximate location of the *Magistrale* [1993] seismicity swarms in San Diego Bay, and the yellow star marks the approximate epicenter of the 1933 Long Beach earthquake. (b) Inset of the San Onofre stepover. (c) Inset of the Carlsbad Canyon stepover. (d) Inset of the Torrey Pines stepover.

northwest from La Jolla Canyon, cutting the outer shelf and continental slope from La Jolla to Newport Beach, where the fault steps back onshore. The fault parallels the coast from Newport Beach to Seal Beach and continues to the northwest into the Los Angeles Basin.

The 1933 *M* 6.4 Long Beach earthquake is the most recent major event on the NIRC fault zone, with rupture on the northern end of the NIRC fault zone. Instrument recordings show that rupture was entirely onshore near Newport Beach, with propagation to the north [*Hauksson and Gross*, 1991]. No surface rupture was observed for this event [*Wood*, 1933].

As the majority of the NIRC fault zone is offshore, paleoseismic observations and slip rate estimates are limited to the southernmost and northernmost onshore sections. On the southern NIRC near San Diego, the paleoseismic history and fault slip rate are constrained from trenching studies near Mission Beach and Mount Soledad. From these studies, the slip rate is estimated at 1.0–2.0 mm/yr [*Lindvall and Rockwell*, 1995; *Rockwell*, 2010]. The most recent event is dated at 1650 ± 120 A.D., following an estimated 5.5 kyr period of quiescence [*Lindvall and Rockwell*, 1995; *Rockwell*, 2010]. Earthquake clustering is observed in five events prior to the quiescence, with these events occurring between approximately 6 and 9.3 ka [*Rockwell*, 2010]. Near La Jolla, the most recent event exhibits approximately 3 m of slip on one strand [*Rockwell*, 2010]. *Grant and Rockwell* [2002] hypothesize that this event could have been part of a larger throughgoing rupture or rupture sequence that may have included the Agua Blanca fault to the south in Mexico and perhaps some offshore segments of the NIRC fault zone. On the northern section of this fault zone, *Grant et al.* [1997] estimate the slip rate on the Newport-Inglewood fault to be 0.35–0.55 mm/yr based on cone penetration tests (CPTs), and *Freeman et al.* [1992] propose a rate of 0.5 mm/yr based on oil well logs, CPTs, borings, and seismic reflection data. The CPT data of *Grant et al.* [1997] indicate that the northern NIRC has hosted at least three and as many as five ruptures since 11 ka.

Offshore knowledge of the fault geometry is incomplete, particularly near or on the continental shelf where there is a dearth of seismic data, and there are no estimates of slip rate. Slip rates for the

offshore NIRC fault zone have not been estimated, largely due to the lack of core data to constrain the age of offset stratigraphic horizons and the absence of clearly defined piercing points. No major historic earthquakes have been documented on the offshore NIRC fault. Although past studies have described the NIRC fault geometry and segmentation, the distribution of offshore seismic surveys is limited, the data density is not uniform, and there remains a dearth of data on or close to the continental shelf resulting in gaps in fault mapping. Previous studies describe several main strands or segments to the NIRC fault zone and three main segment boundaries, by Del Mar/Torrey Pines, Carlsbad Canyon, and San Onofre [*Hogarth et al*., 2007; *Ryan et al*., 2009]. They note, however, that it is often difficult to carefully map shallow deformation due to overprinting and masking of shallow structure by the active-source seismic source signature.

Where available, records of offshore seismicity provide additional information regarding the fault geometry and state of stress. *Magistrale* [1993] analyzed three earthquake swarms that occurred near the southern NIRC segment in San Diego Bay between 1985 and 1987. In this region, the NIRC strikes NNW and dips to the southwest (~70°). The hypocenter locations of these swarms form southwest dipping clusters that are elongated in the northeast-southwest direction, and focal mechanisms for these events indicate slip on northeastward striking structures. *Magistrale* [1993] proposed that these clusters occurred where northeasterly striking faults near Point Loma intersect with the southwestward dipping NIRC fault plane, and that the occurrence of these events indicated a change in stress on the fault. *Grant and Shearer* [2004] analyzed offshore microseismicity in the central region of the fault using a method that improves the relative locations of events within clusters and thus increases the reliability of spatial trends and alignments. They focused their attention on two main clusters that correlate with mapped NIRC fault traces within the events' location uncertainty: one cluster 10 km north of Oceanside in 1981 and a second cluster near Newport Beach in 2000. Both clusters occurred on a NNW striking, nearly vertical fault plane, consistent with previous mapping of the NIRC fault zone.

3. Methods

3.1. Seismic Reflection Data

Fault imaging and geomorphic mapping were performed using nested seismic reflection data at four different resolutions, as well as high-resolution (25 m pixel resolution) multibeam bathymetric data [*Dartnell et al*., 2015]. Seismic reflection data included a 1979 Chevron multichannel seismic (MCS) data set reprocessed by Geotrace using a prestack time migration approach, a 2006 U.S. Geological Survey (USGS) single-channel seismic (SCS) data set [*U.S. Geological Survey Coastal and Marine Geology Program*, 2006] reprocessed in-house (details below), acoustic Compressed High Intensity Radar Pulse (CHIRP) data collected between 2006 and 2009, and newly acquired high-resolution 2-D MCS data collected in August 2013 using a sparker source. The location of these surveys is shown in Figure 2. The CHIRP and USGS data image the top strata and resolve the most recent episodes of deformation. The Chevron MCS data image the deeper structure and interconnectivity of fault splays, while the 2013 sparker MCS data provide high-resolution imaging of intermediate stratal depths.

The 1979 Chevron MCS data were acquired with a 96-channel hydrophone streamer with 33.5 m hydrophone receiver spacing and shot spacing. This yielded 48-fold data with a common midpoint space of 16.75 m of separation. The source was a 49.2 L (7620 cm^3) air gun array. The penetration depth of these data is ~2 s two-way travel time (TWTT) or ~2 to 3 km depths. These data were reprocessed by Geotrace, using a hybrid multiple suppression scheme (surface-related multiple elimination (SRME), plus Radon filtering), trace interpolation in shot and receiver space, and prestack time migration [*Driscoll et al*., 2013].

The 2006 USGS SCS data were collected with a single-channel receiver and a 2 kJ minisparker source. Reflectors are resolvable down to ~1 s TWTT or ~1 km. The original data set contained moderate levels of noise and strong multiples. To improve resolution and aid in interpretation, reprocessing was performed in-house. Methods included swell removal, source signature shaping, multiple removal, and coherency filtering to improve reflector continuity [*Sargent et al*., 2011]. Shaping of the source wavelet was performed in the frequency domain converting the source signature to zero phase and reducing a prominent notch due to surface ghosts. Multiple removal was performed using a 1-D version of SRME [*Berkhout and Verschuur*, 1997; *Riley and Claerbout*, 1976; *Verschuur and Berkhout*, 1997]. The 1-D assumption works well in regions with low slope (i.e., continental shelves) but has suboptimal results on steeper areas such as the continental slope. Figure 3

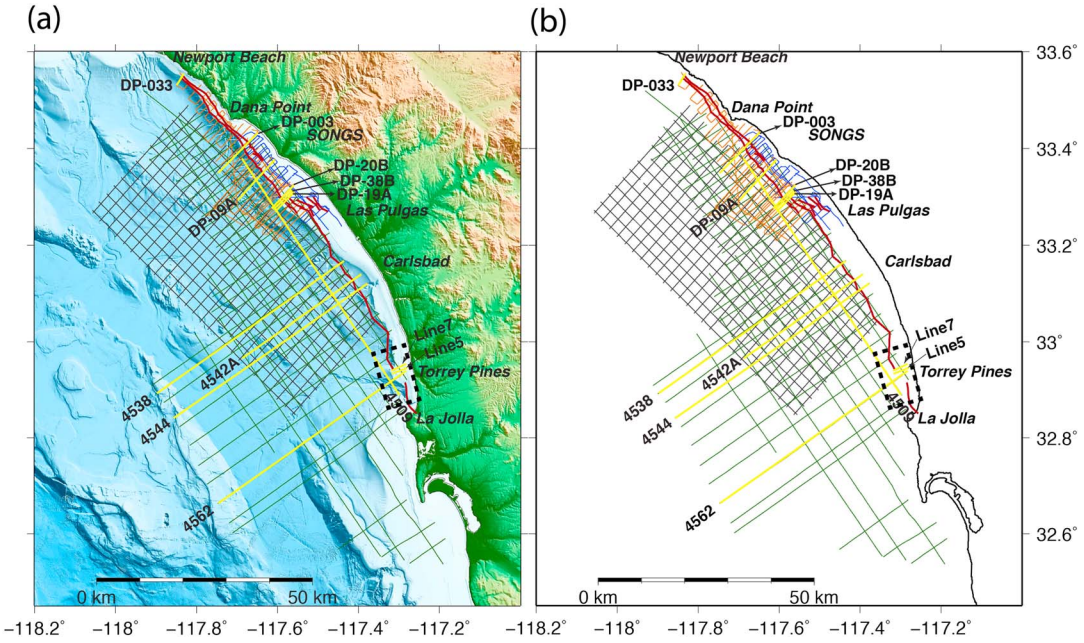

Figure 2. Track line map showing the location of seismic reflection profiles used in this study. (a) With bathymetry and topography plotted and (b) without bathymetry or topography. The green lines are from the reprocessed 1979 Chevron MCS survey, the black lines are from the 2013 MCS surveys, the orange lines are from the 2006 SCS USGS survey, and the blue lines are from the SIO CHIRP surveys. The red line denotes the NIRC fault. Landmarks are noted on the figure. Profiles presented in this paper are highlighted in yellow and labeled by line name. The black dashed box shows the approximate location of the *Hogarth et al.* [2007] study. Line DP-09A is in Figure 3; lines 4562 and 4509 are in Figure 4; line 7 and line 5 are in Figure 5; lines 4544, 4542A, and 4538 are in Figure 6; lines DP-19A, DP-38B, and DP-20B are in Figure 7; and lines DP-033 and DP-003 are in Figure 11.

shows an example of the difference between original and reprocessed data on USGS line DP-09 that illustrates the filter performance. Coherency filtering was performed on overlapping patches of 250 traces and 0.05 s using an estimate of local dip and least squares trace estimation [*Yilmaz*, 2001].

All CHIRP surveys were conducted with the Scripps Institution of Oceanography's Edgetech SUBSCAN profiler, with coincident transducer and receiver arrays. The instrument was operated using a 50 ms swept pulse of 0.7–3.0 kHz or 1–6 kHz depending on sediment character, resolving stratigraphy to a depth of approximately 50 m.

The 2013 MCS data were collected offshore on the R/V *New Horizon* and R/V *Melville* using a 2 kJ three-tip EG&G 402–7 sparker source and 48-channel streamer, with a group spacing of 6.25 m and 6.25 m shot spacing, allowing reflectors to be resolved to approximately 1.5 s two-way time or 1.5 km depth. These data were stacked at 1500 m/s, and further processing included poststack *f-k* migration using a nominal water velocity of 1500 m/s [*Driscoll et al*., 2013].

Some lines in each of these data sets intersect the NIRC fault zone. The new sparker, USGS, and CHIRP data cross the NIRC fault on the widest part of the shelf offshore San Onofre Nuclear Generating Station (SONGS), but north of SONGS where the shelf is narrow only the CHIRP and USGS data cross the fault. When combined, this is a multiresolution data set of unparalleled density and distribution that can be used to constrain fault architecture and identify episodes of deformation on the NIRC fault zone.

3.2. Coulomb Stress Modeling

Models of total Coulomb stress change were conducted for each fault strand in an attempt to develop a quantitative understanding of static triggering and the potential for throughgoing rupture across fault stepovers. There are many factors that contribute to the likelihood of throughgoing rupture across stepovers, perhaps dynamic triggering serving as one of the largest. Nevertheless, models of static stress change can serve as an additional constraint to complement empirical studies. It should be noted that static stress change cannot capture the factors that govern interactions in the system during rupture

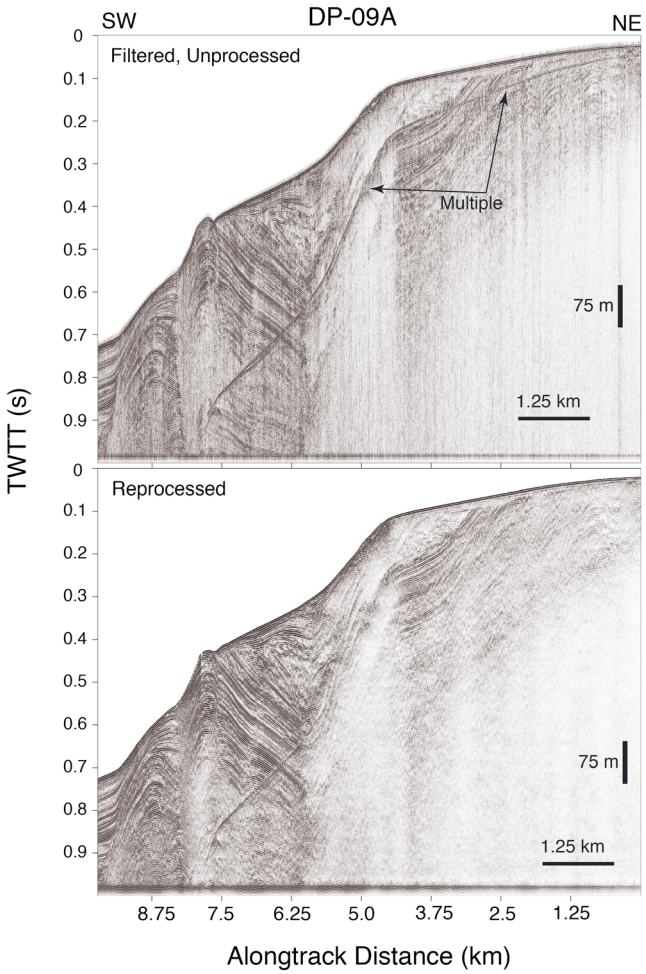

Figure 3. Example of the improvements after reprocessing the 2006 USGS SCS data, line DP-09A. (top) The original band-pass-filtered data and (bottom) the reprocessed data. Note that the multiple has been suppressed in all locations except the steeply dipping regions. The continuity of reflectors and signal-to-noise ratio have been improved.

propagation, such as rupture directivity, clamping, and unclamping; to quantify these effects, fully dynamic stress simulations would need to be computed. This stress change modeling was conducted using hypothetical, homogeneous slip distributions on each strand and was performed using the USGS package, Coulomb 3 [*Lin and Stein*, 2004; *Toda et al.*, 2005; *Toda et al.*, 2011]. Here the 3-D fault surfaces interpreted from the reflection data were simplified to planes with strike and dip determined as the average of the observed faulting surface (Table 1). In this modeling approach "source" faults that are assigned uniform slip impart stress on the surrounding medium and other nearby "receiver" faults with prescribed location, strike, and dip. Calculations are made in a two-dimensional elastic half-space, using uniform isotropic material properties, and following the method of *Okada* [1992]. For this study, the total Coulomb stress change was calculated, treating each fault segment individually as a source fault and then determining the stress change on the neighboring receiver fault segments. A total of 20 computations were performed to model the stress changes for each source and receiver fault geometry pair. The computational domain was a Cartesian grid of 0.5 km in x and y and 1 km in depth. The material properties were prescribed with a Poisson's ratio of 0.25, static frictional coefficient 0.4, and Young's modulus of 75 GPa. The Young's modulus was derived from the Poisson's ratio and a shear modulus of 30 GPa. The shear modulus was derived from a one-dimensional profile of compressional and shear wave speed near Oceanside that was extracted from the three-dimensional structure model for Southern California Earthquake Center Community Velocity Model–Harvard (SCEC CVM-H) [*Shaw et al.*, 2015].

Table 1. Strand Geometry Used in the Coulomb Stress Modeling

Strand	Strand Length (km)	Average Strike (deg)	Average Apparent Dip (deg)
La Jolla	8.1	337	63°SW
Torrey Pines	19.6	338	87°SW
Carlsbad Canyon	27.4	324	85°NE
Camp Pendleton	42.3	320	89°NE
Dana Point	27.6	317	85°NE

4. Results and Observations

4.1. Geometry of the Offshore NIRC Fault Zone StepOvers

The primary observations from this study suggest that the NIRC exhibits a relatively continuous fault trace, except for three distinct stepovers offshore as outlined by yellow boxes and insets in Figure 1, and an additional strand that parallels a main trace for ~20 km off the

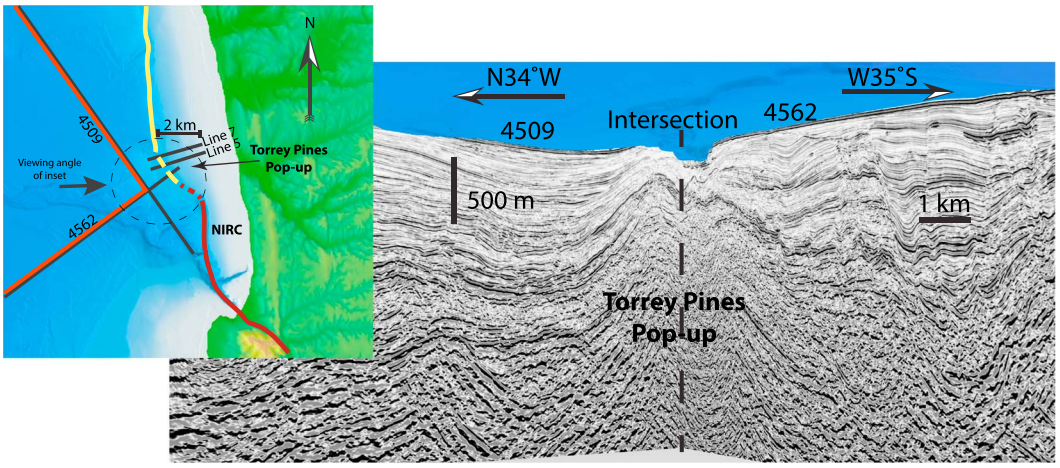

Figure 4. An image of the southernmost Torrey Pines stepover. (left) The map view shows the location of the pop-up and the location of the Chevron lines shown in the figure (profile location also shown in Figure 2). The yellow line is the Torrey Pines strand of the NIRC trace, and the red is the La Jolla strand. The dashed circle shows the approximate extent of the pop-up structure. (right) The image shows the pop-up in the deeper Chevron data created by the step over, with a horizontal look angle toward the intersection of the line. The dashed black line shows the intersection of Chevron lines 4509 and 4562 for clarity. The arrows indicate the strike of each seismic line. The red lines show the location of the seismic profiles, and the arrow shows the viewing angle. These data extend to approximately 2–3 km depth. Note that the reflectors are deformed in an anticlinal formation at the pop-up structure. The location of lines 7 and 5 shown in Figure 5 is denoted.

coast of Dana Point. In this study, stepover width is defined as the minimum distance between two strands. The stepovers separate the fault into four main strands, which from south to north, are here named the La Jolla strand, the Torrey Pines strand, the Carlsbad Canyon strand, and the Northern strand that includes the Camp Pendleton splay and Dana Point splay (Figure 1).

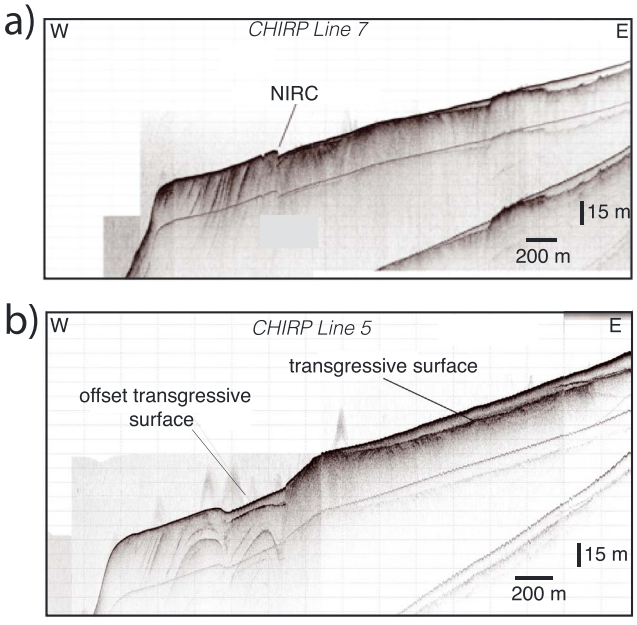

Figure 5. High-resolution CHIRP profiles across the Torrey Pines pop-up. Location of profiles is shown in Figures 2 and 4. (a) Line 7 images the NIRC fault and demonstrates the seafloor deformation observed in the southern NIRC fault zone. (b) Line 5 images a basin formed by NIRC splays in a distributed zone of faulting within the stepover.

The southernmost stepover occurs at a compressional left step in faulting offshore of Torrey Pines (Figure 1). This stepover, referred to as the Torrey Pines stepover, is approximately 2 km in width, as shown in map view in Figure 4 (uninterpreted seismic profile is shown in Figure S1 in the supporting information). It is associated with a compressional pop-up structure and occurs at the location where the shelf is wide along the southern coast, north of La Jolla canyon (Figure 1). The pop-up structure is imaged in the deeper Chevron data down to approximately 1.5 km depth (Figure 4) and also in the shallow CHIRP data (Figure 5). Figure 4 demonstrates the uplift and antiformal structure in the deeper strata. Line 4562 crosses the NIRC fault and is observed on the section; however, it is blocked from view in this fence diagram because of the intersection with line 4509. Figure 5 presents the direct imaging in CHIRP data of the NIRC fault offsetting the uppermost strata and transgressive surface on the

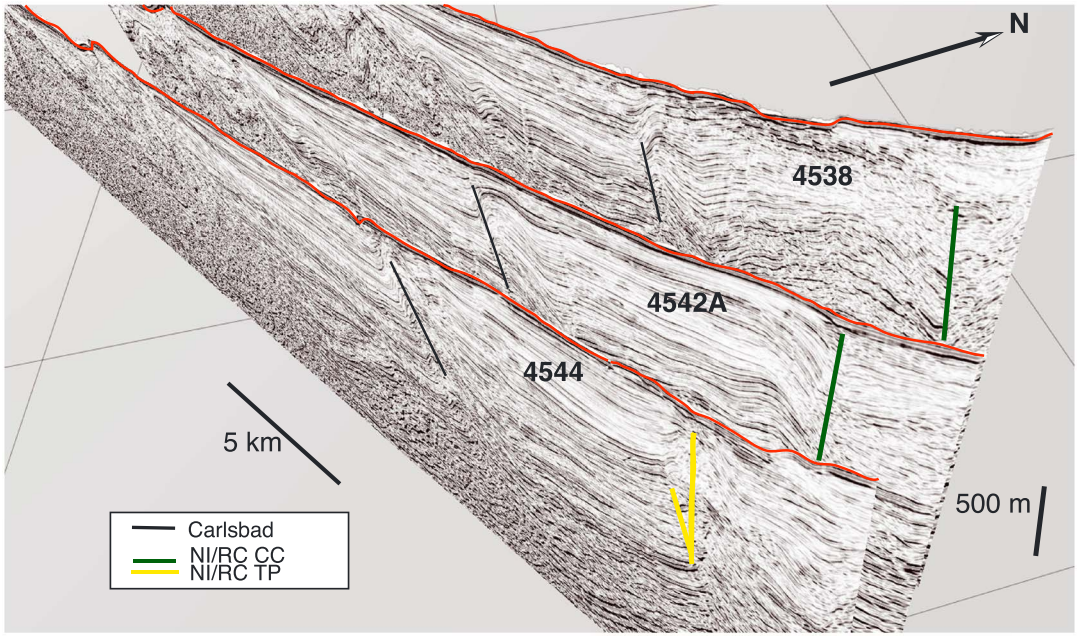

Figure 6. An image of the Carlsbad Canyon stepover. Moving north this stepover is characterized by a slight westward step (see Figure 8), as well as a change in the recency of deformation. The north direction is marked. The three Chevron MCS profiles cross the NIRC fault zone and the Carlsbad trend to the west (see Figure 2 for the profile locations). The red line denotes the seafloor, the yellow line marks the Torrey Pines strand of the NIRC fault on line 4544, the green lines mark the Carlsbad Canyon strand of the NIRC fault on lines 4542A and 4538, and the black lines mark the Carlsbad trend (fault near the base of the slope). Note that deformation extends almost to the seafloor on 4544 and is progressively deeper to the north. The NIRC geometry also transitions from a slight eastward dip on the Torrey Pines strand to a more westerly dip on the Carlsbad Canyon strand.

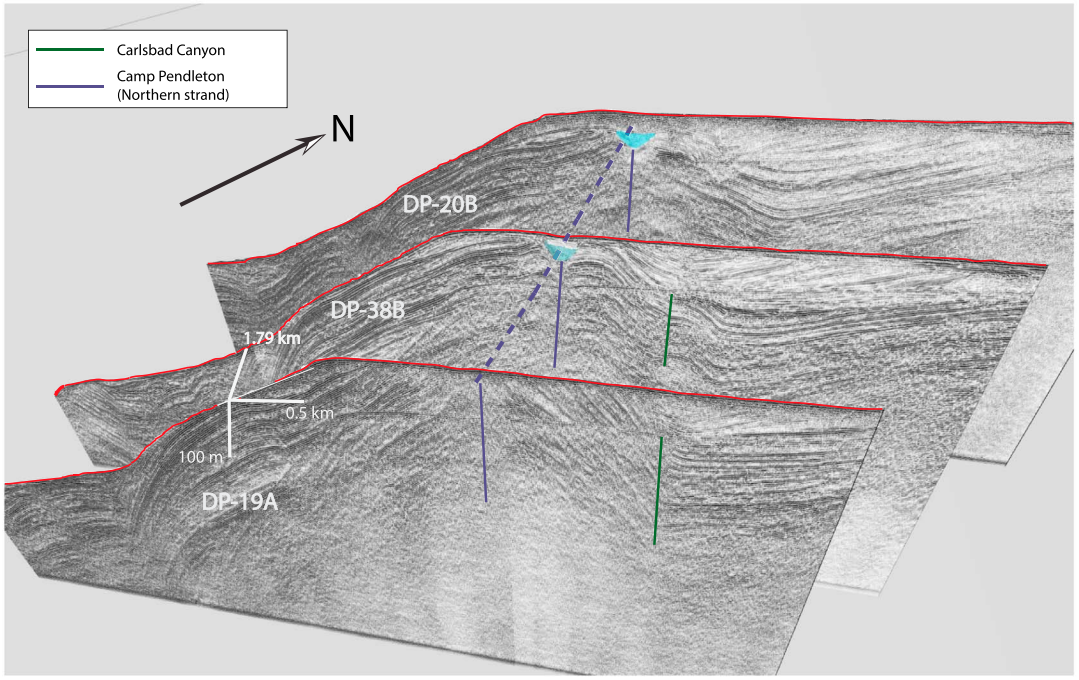

Figure 7. A perspective view of the third step over located offshore San Onofre. USGS lines, DP-19A, DP-38B, and DP-20B, are shown (see Figure 2 for the profile locations). North direction and scale are shown. The purple and green lines show the Camp Pendleton and Carlsbad Canyon strands of the NIRC fault, respectively. The purple dashed line shows the inferred structural trend between profiles. The location of a paleochannel is highlighted in blue. The red lines denote the seafloor on each profile.

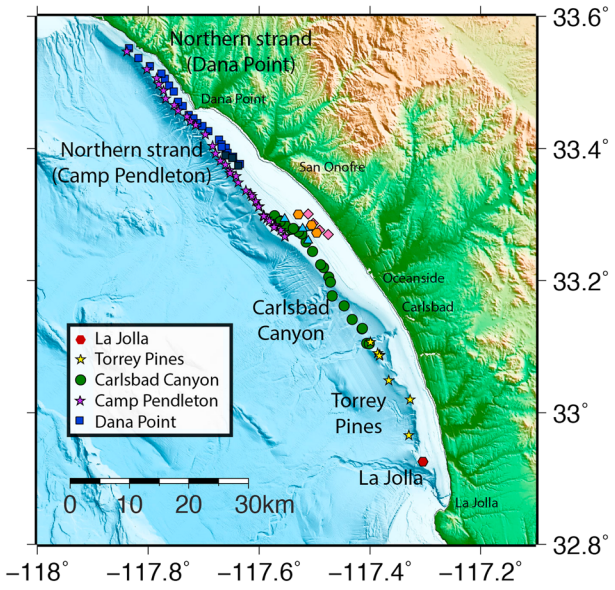

Figure 8. Locations of NIRC fault zone as observed in seismic profiles. The colored symbols represent all mapped segments and splays as follows: red hexagons, La Jolla strand; yellow stars, Torrey Pines strand; green circles, Carlsbad Canyon strand; purple stars, Northern strand, Camp Pendleton splay; blue squares, Northern strand, Dana Point splay. In the south, the La Jolla strand is mapped from seafloor geomorphic expression in multibeam bathymetry, as well as the mapping of *Hogarth et al.* [2007].

shelf. The transgressive surface is an erosional surface, formed by the last rise in sea level, ~8–11 ka; as such, it can be used as a rough datum for the most recent episode of deformation. The top plot in Figure 5 shows the presence of an eastward facing fault scarp on CHIRP line 7. The bottom plot shows a small pull-apart basin that is superposed on the larger pop-up structure with penetration to ~50 m subbottom depth.

The second major stepover, referred to as the Carlsbad stepover, occurs offshore Carlsbad, where the NIRC fault crosses Carlsbad Canyon (Figure 1). This step over is less than 0.5 km in width, and strata within the stepover exhibit slight compressional deformation. This step is characterized by a slight left step between the Torrey Pines and Carlsbad Canyon strands of the fault. Minor changes in strand strike and dip, and most notably, by a change in the recency of deformation are observed in the seismic data to the north and south of the step over. Figure 6 shows three Chevron MCS lines labeled 4544, 4542A, and 4538 that cross the trend of the NIRC fault near the Carlsbad step (uninterpreted seismic data are shown in Figure S2). Line 4544 crosses the Torrey Pines strand south of the stepover, and lines 4542A and 4538 cross the Carlsbad Canyon strand north of the step. North of line 4544, the NIRC fault steps to the west, and the dip changes from a slight eastward dip on the northernmost Torrey Pines strand, to a slight westward dip on the southernmost Carlsbad Canyon strand. The Carlsbad Canyon strand is different in stratigraphic nature from the Torrey Pines strand. Most observations of the fault along the Carlsbad Canyon strand demonstrate a more fractured nature, as well as transtension evidenced by reflectors collapsing toward the fault. In contrast, the Torrey Pines strand shows a very clear fault boundary deforming the seismic reflectors and stratigraphic layers. Additionally, the thickness of the sediment package mantling the NIRC fault increases to the north of the stepover. In this regard, reflector offset is observed shallower in the Torrey Pines strand (line 4544) than the Carlsbad Canyon strand (lines 4542A and 4538). The Carlsbad step is located in the only region where the NIRC fault zone is not adjacent to the shelf break (Figure 1).

The third major step over is offshore between Las Pulgas Road and San Onofre along the widest section of the shelf between La Jolla and Newport Beach (Figure 1). This step over is referred to as the San Onofre step over. It is less than 1 km in width, and it exhibits a compressional architecture. The geometry of the step is displayed in three USGS lines, DP-19A, DP-38B, and DP-20B shown in Figure 7 (uninterpreted seismic data are shown in Figure S3). The Carlsbad Canyon strand and Camp Pendleton splay of the Northern fault strand are shown by the green and purple lines, respectively. The Carlsbad Canyon strand and Camp Pendleton splay are separated by a left step of approximately 1 km. The Carlsbad Canyon fault strand terminates northward, and the westward Camp Pendleton splay of the Northern fault strand terminates southward as the two overlap (Figure 7). The Carlsbad Canyon strand curves to the northwest, forming an anticlinal feature on the shelf, which is crosscut by the Camp Pendleton splay (Figure 7). This anticlinal feature appears to be responsible for forming the wide shelf in this region, as it traps sediment from the east. It should also be noted that here, the Camp Pendleton splay appears to control the location of a paleochannel, marked in blue in Figure 7. The faults and antiformal structure are also observed in 3D MCS data on the shelf as presented by *Holmes et al.* [2014].

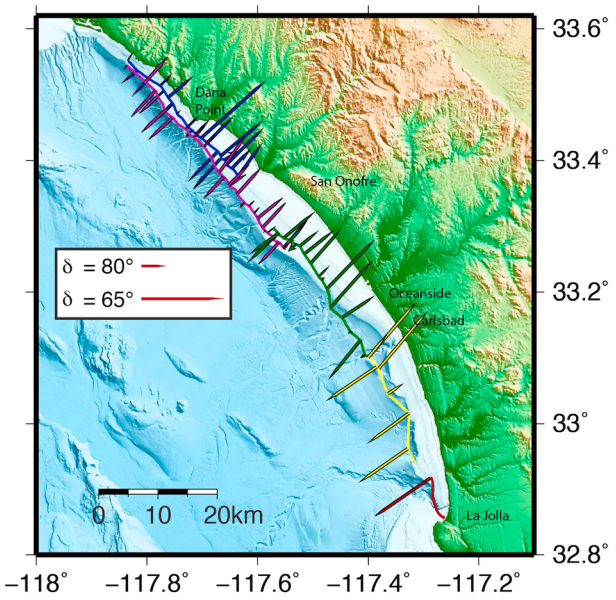

Figure 9. Map of apparent dips of the five main segments, from seismic lines crossing the NIRC fault zone. Red, La Jolla strand; yellow, Torrey Pines strand; green, Carlsbad Canyon strand; purple, Northern strand, Camp Pendleton splay; blue, Northern strand, Dana Point splay. The longer lines indicate a shallower dip; the shorter lines indicate vertical or near-vertical dips.

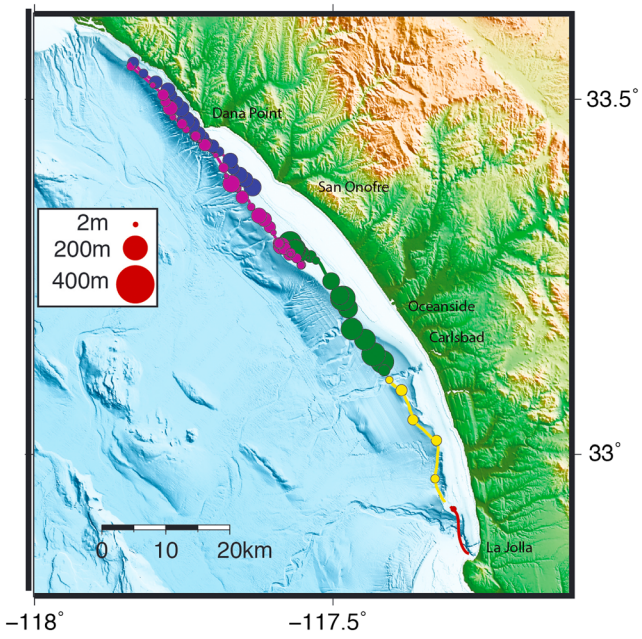

Figure 10. Map of the depth of deformation along each strand, from seismic lines crossing the NIRC fault. The circle size represents the shallowest depth of deformation below the seafloor. The circle diameter is defined on a log scale; 2 m or less, 200, and 400 m are shown in legend. Red, La Jolla strand; yellow, Torrey Pines strand; green, Carlsbad Canyon strand; purple, Northern strand, Camp Pendleton splay; blue, Northern strand, Dana Point splay.

North of the San Onofre step over, the NIRC fault is composed of two subparallel splays of what is referred to as the Northern strand. The longer western structure is referred to here as the Camp Pendleton splay, and the eastern structure is referred to as the Dana Point splay (Figure 8). Both the Camp Pendleton and Dana Point splays approach Newport Beach onshore (Figures 1 and 8), and are spaced approximately 200 m to 2 km apart, depending on the location along strike. At the southern end of this strand, the two splays are spaced farther apart, closer to 2 km; toward the northern end and the central region, they are much closer together. The two strands do not merge at depths less than ~2 km as imaged by the seismic data, but may coalesce at greater depths, past the penetration depth of the seismic data. The deeper geometry is not determinable from the imaged depths. In the shallow data however, there are many locations in which the splays share a similar dip direction or dip toward each other.

4.2. Geometry of the NIRC Fault Zone: Strands and Characteristics

Figure 8 shows the location of the NIRC fault zone based on the survey lines shown in Figure 2. The various colors and symbols denote the separate strands and splays mapped here, with the four main named strands (and splays) labeled in the legend: the La Jolla strand, Torrey Pines strand, Carlsbad Canyon strand, and Northern strand composed of the Camp Pendleton and Dana Point splays. The short, discontinuous splays observed in Figure 8 near San Onofre may continue to the north or south, but the data employed in this study do not image them any farther; thus, they are not discussed at length or included in stress modeling. It should be noted, however, that this is the only known location where the NIRC fault zone is represented by such a large number of smaller splays, as opposed to being concentrated on

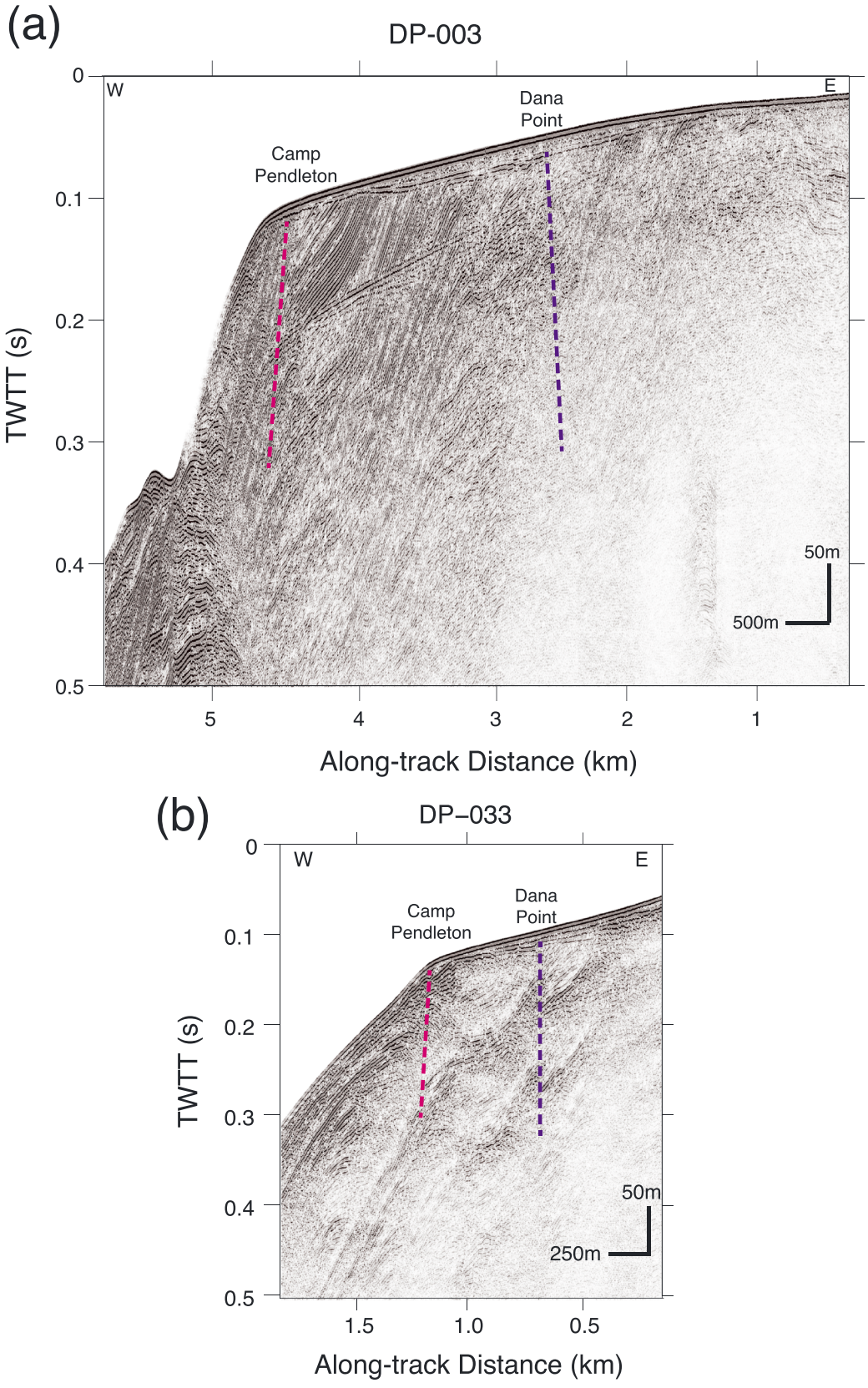

Figure 11. USGS lines DP-003 and DP-033, with the Camp Pendleton and Dana Point splays denoted in pink and purple, respectively.

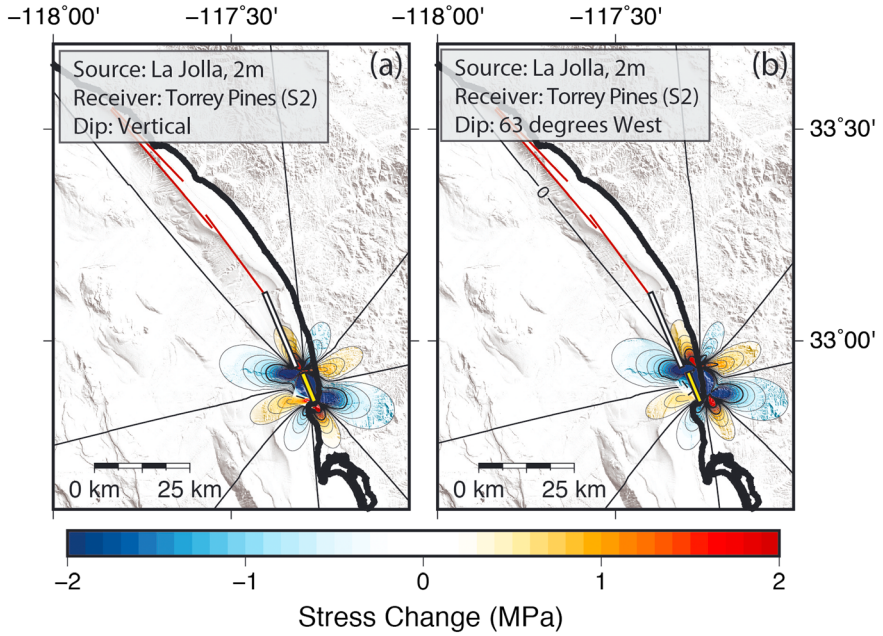

Figure 12. Effect of fault dip on total Coulomb stress change from 2 m of slip on a source fault (marked by yellow bar) onto receiver fault (marked by a white bar). (a) Stress change onto the Torrey Pines strand with 2 m of displacement on a vertical La Jolla strand. (b) Stress change onto the Torrey Pines strand, from 2 m of displacement on a dipping La Jolla strand (apparent dip 63°WSW), as observed in seismic data.

one or two main strands. The strike of each fault strand varies along its length, and fault strands in the north of the study region generally exhibit a more northwesterly strike. Additionally, the fault defines or follows the shelf edge for the majority of the margin. To the south of the Torrey Pines pop-up structure, the location of the NIRC fault zone is based on data presented in *Hogarth et al.* [2007].

The NIRC fault dip varies significantly along strike as well as between strands. Figure 9 summarizes the apparent dip mapped for each of the four main strands and splays, plotted with the same color scheme as Figure 8. Short lines indicate a near-vertical dip, whereas longer lines indicate a shallower dip. Some strands, such as Carlsbad Canyon strand, display a more consistent dip along strike, in this case a consistent northeastwardly dip. In other strands, such as the Camp Pendleton splay, the fault plane appears to be closer to vertical. The dip of the Camp Pendleton and Dana Point splays of the Northern strand varies from both dipping in the same direction (the southern section of the Northern strand) to generally dipping away from each other on the northern section of the Northern strand.

The depth of deformation along the NIRC fault zone varies along strike. South of the Carlsbad Canyon step, the NIRC fault zone deformation extends to or close to the seafloor (Figure 10). North of Carlsbad Canyon, the deformation is observed deeper in the seismic data until near Las Pulgas Road. From Las Pulgas Road to Dana Point, the deformation is typically confined to be beneath the transgressive surface and in some locations deforms it. In areas where the transgressive surface shoals, it correlates with the NIRC fault zone and the Cristianitos fault. Nevertheless, the preferred hypothesis from other studies is that these are antecedent features that are more resistant to erosion and do not record deformation of the transgressive surface per se [*Klotsko et al.*, 2015]. North of Dana Point, the NIRC fault deformation offsets the transgressive surface (dated at ~8–11 ka) in some locations and in regions approaches the seafloor. To the south of the Carlsbad Canyon stepover, the deformation is close to or at the seafloor (Figure 10). Moving north in the central section of the NIRC fault zone (Carlsbad Canyon strand, as well as the southern section of the Camp Pendleton splay of the Northern strand) the average deformation steps deeper, until the region around San Onofre on the widest section of the shelf. Moving northward toward Dana Point, the average deformation progressively extends to shallower depths once again. Two USGS seismic lines are plotted with interpretations in Figure 11 to show the vertical extent of deformation along some of the northern lines imaging the Camp Pendleton and Dana Point splays (uninterpreted

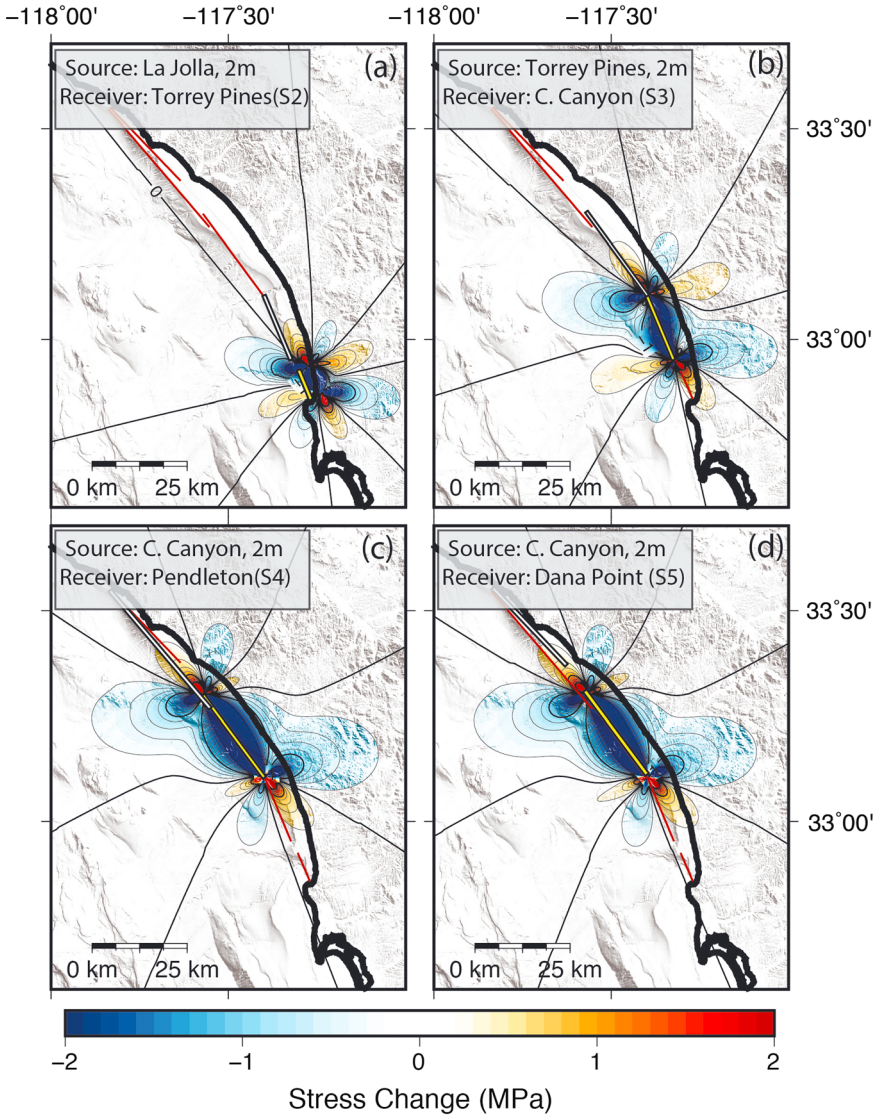

Figure 13. Motivation of rupture scenario I—Coulomb stress change from 2 m of displacement on source faults with rupture on the southernmost La Jolla segment. The yellow bars indicate the source fault, and the white bars indicate the receiver fault. S2, S3, S4, and S5 represent the numbers of each receiver faults. (a) Total stress change on the Torrey Pines receiver fault (S2) from the La Jolla source fault. (b) Total stress change onto the Carlsbad Canyon receiver fault (S3) from the Torrey Pines source fault (S2). (c) Total stress change onto the Camp Pendleton receiver fault (S4) from the Carlsbad Canyon source fault (S3). (d) Total stress change onto the Dana Point receiver fault (S5) from the Carlsbad Canyon source fault (S3).

data are shown in Figure S4). Here the deformation appears to extend near the surface and appears to offset the transgressive surface.

4.3. Results of Coulomb Stress Change Modeling

The suite of static Coulomb stress change models presented below is a synopsis of an effort to support quantitatively empirical observations of stepover width allowing or inhibiting rupture to propagate across stepovers and aid in determining which of all possible rupture scenarios are more or less likely. These models employ the material properties listed in section 3, as well as the fault geometries described in Table 1. The total Coulomb stress change was computed from each strand as a source fault to each other respective strand as a receiver fault, resulting in a total of 20 models. In each model, 2 m of coseismic dextral slip was prescribed on the source fault, assumed as a conservative upper bound for coseismic slip, based on past coseismic deformation observed on the NIRC fault in onshore paleoseismic trenches [*Lindvall and Rockwell*, 1995]. Coulomb failure stress was computed at 6 km depth as this is

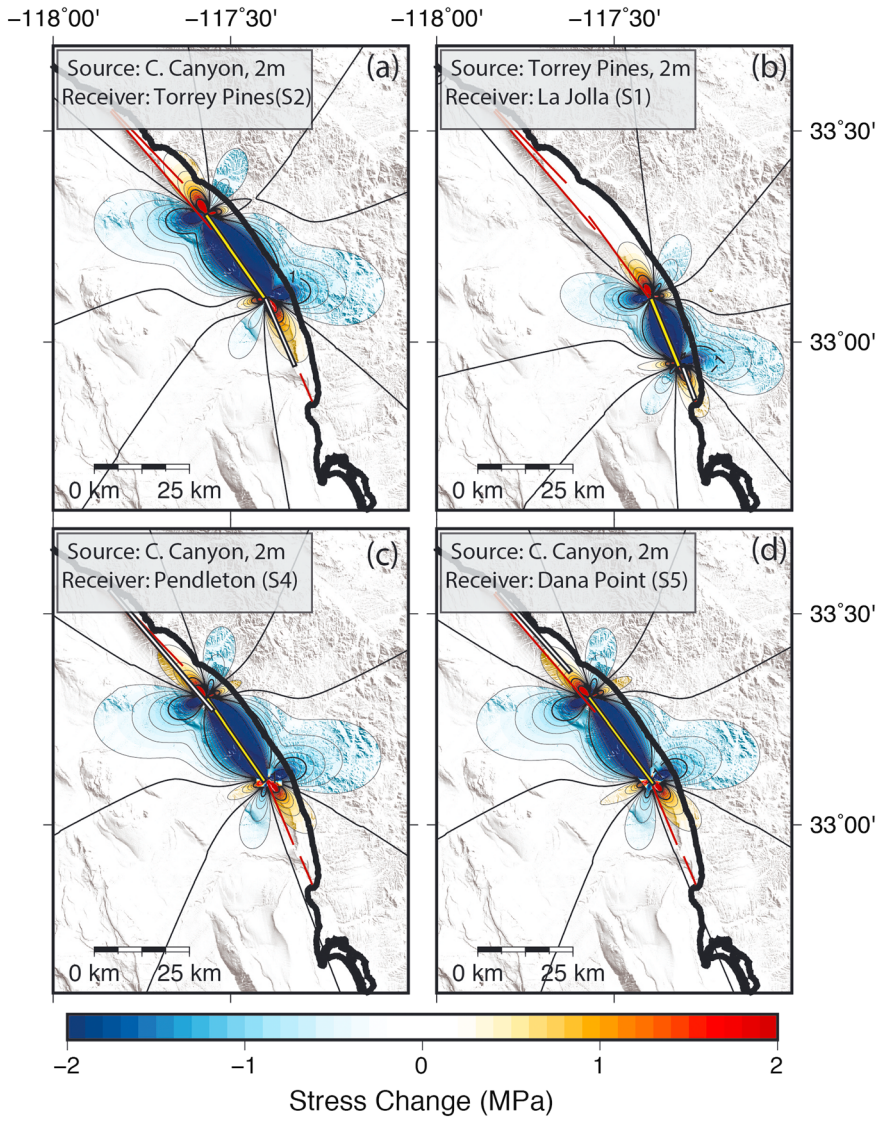

Figure 14. Motivation of rupture scenario II—total Coulomb stress change from 2 m of displacement on the Carlsbad Canyon strand (marked by yellow bar), with stress change northward and southward onto adjacent receiver faults (marked by a white bar). (a) Stress change on the Torrey Pines receiver fault (S2) from rupture on the Carlsbad Canyon source fault (S3). (b) Stress change onto the La Jolla receiver fault (S1) from the Torrey Pines source fault (S2). (c) Stress change onto the Camp Pendleton receiver fault (S4) from the Carlsbad Canyon source fault (S3). (d) Stress change onto the Dana Point receiver fault (S5) from the Carlsbad Canyon source fault (S3).

approximately the middle of the seismogenic zone, assuming that the fault plane extends to the base of the seismogenic zone in this region, ~10–15 km depth [*Astiz and Shearer*, 2000]. The geometries of each fault strand input to the models of static stress change (strike and apparent dip) are recorded in Table 1, determined as the strike and average dip along each mapped strand.

Figures 13–15 each describe a potential rupture scenario, with the four plots in each figure illustrating the stress change assuming consecutive rupture, meaning rupture through multiple strands in a single event. However, considering that these are static stress models, they also are worth considering in terms of the likelihood of a sequence of separate events. The scenarios describe the effect rupture on one entire strand would have on the nearby strands. Each plot shows the stress change from a source fault, marked with a yellow bar, onto a receiver fault, denoted by a white bar. In the figures, the La Jolla strand is labeled as S1, Torrey Pines as S2, Carlsbad Canyon as S3, Northern strand/Camp Pendleton as S4, and Northern strand/Dana Point as S5.

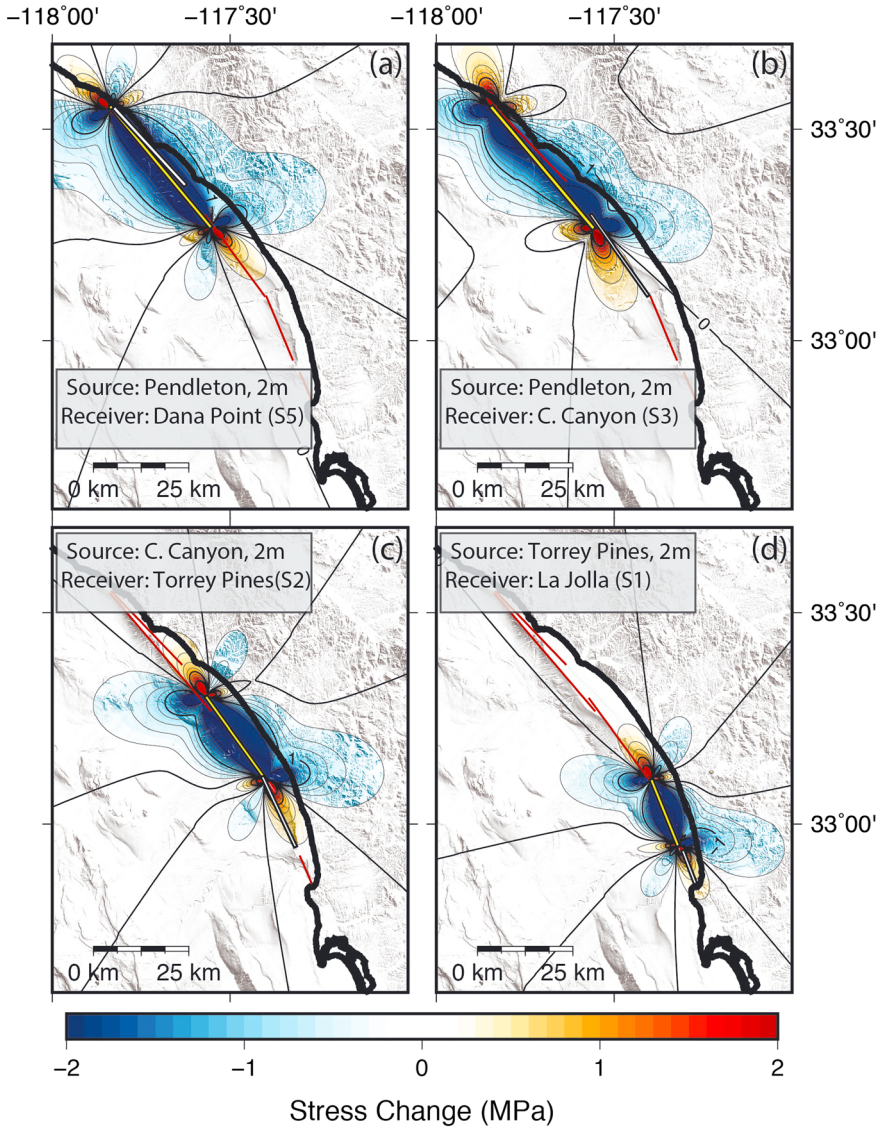

Figure 15. Motivation of rupture scenario III—Coulomb stress change from 2 m of displacement starting on the Camp Pendleton source fault (yellow bar). Receiver segments marked by white bars. (a) Stress change on the Dana Point receiver fault (S5) from the Camp Pendleton source fault (S4). (b) Stress change on the Carlsbad Canyon receiver fault (S3) from the Camp Pendleton source fault (S4). (c) Stress change on Torrey Pines receiver fault (S2) from the Carlsbad Canyon source fault (S3). (d) Stress change on the La Jolla receiver fault (S1) from the Torrey Pines source fault (S2).

Figure 12 demonstrates the effect of fault dip on Coulomb stress change across a stepover. The La Jolla segment exhibits an apparent dip of 63°WSW. The total Coulomb stress change on the Torrey Pines segment from deformation on the La Jolla strand is small, given the observed dips of each of these strands (Figure 12b). If the La Jolla strands were assumed to be vertical, however, the Torrey Pines strand would experience a significant increase (greater than 2 MPa) in stress (Figure 12a).

The first scenario, Scenario I, investigates the effects from rupture on the La Jolla strand (S1) on strands to the north (Figure 13). Figure 13a shows the stress change from the La Jolla strand (yellow bar) onto the Torrey Pines strand (S2; white bar). The main increase in Coulomb stress is east of the receiver fault. In fact, the southern terminus of the Torrey Pines strand is in an area of reduced or no Coulomb stress change. Assuming that rupture continues northward, slip on the Torrey Pines strand causes an increase in Coulomb stress on the Carlsbad Canyon receiver fault (Figure 13b). Rupture on the Carlsbad Canyon source fault causes the maximum increase in Coulomb stress to be slightly east of the Camp Pendleton receiver fault (Figure 13c) and the maximum to be slightly west of the Dana Point receiver fault (Figure 13d).

In Scenario II, rupture occurs on the Carlsbad Canyon strand and affects strands to the north and south (Figure 14). Figure 14a shows the stress change from the Carlsbad Canyon strand (S3) onto the Torrey Pines strand (S2); the Torrey Pines strand is in the middle of the lobe of increased stress. Figure 14b shows that the La Jolla strand experiences increased Coulomb stress as a result of deformation on the Torrey Pines strand. Furthermore, the Carlsbad Canyon strand increases the Coulomb stress on the Camp Pendleton (S4) and Dana Point (S5) strands, up to 1–2 MPa in some locations along strike (Figures 14c and 14d).

Scenario III explores the stress change from rupture on a splay of the northern strand, the Camp Pendleton splay (Figure 15). The Dana Point receiver fault is entirely in the Coulomb stress shadow for rupture on the Camp Pendleton splay source fault (Figure 15a). The Carlsbad Canyon receiver fault has both reduced and increased Coulomb stress for rupture on the Camp Pendleton splay source fault (Figure 15b); it is important to note that the reduced stress is only along the northern terminus of the strand. Despite the strand being on the eastern edge of the increased stress, the central portion experiences a stress increase of almost 2 MPa. Observing the effects southward from the Carlsbad Canyon strand, the Torrey Pines strand is nearly centered in the increased stress lobe as the receiver fault for the Carlsbad Canyon source fault (Figure 15c). Similarly, moving southward from the Torrey Pines strand, the La Jolla strand is in the center of the lobe of increased stress when it serves as the receiver fault to the Torrey Pines source fault (Figure 15d).

5. Discussion

5.1. Mapping and Observations

The results presented in this study suggest that there is a relationship between fault segmentation, and characteristics of margin architecture such as shelf width, and pop-up structures. It also illustrates how the NIRC fault architecture (e.g., dip, strike, and stepover width) may influence rupture along the margin and plays an important role in potential earthquake magnitudes. Along the study area, the shelf is widest by San Onofre. This appears to be caused by an antiformal feature created by a change in strike along the NIRC fault (Figure 7), as well as sediments sequestered or dammed east of this feature that onlap the antiform. The location of a major paleochannel also appears to be controlled by fault location and the anticlines, as the faults may provide areas of weakness. In contrast, the shelf is narrowest by the Carlsbad stepover. Additionally, this study finds, consistent with *Ryan et al.* [2009] and *Maloney et al.* [2016], that the local tectonic setting is often transtensional when the strike of the NIRC fault is more northerly striking and transpressional when more northwesterly striking. For example, the NIRC fault is northwesterly striking in the region of the San Onofre stepover, where the antiformal/transpressional structures are observed. Finally, there are obvious geomorphic and stratigraphic features resulting from the volumetric deformation in stepover regions. For example, the transpressional Torrey Pines stepover results in uplift of the seafloor and significant uplift and doming of reflectors at depth. At the surface, a smaller basin within the stepover is observed at the seafloor; this could be due to a smaller transtensional step over within the Torrey Pines step over, resulting from smaller splay faults, or could perhaps be a reversed-polarity small-scale structure resulting from predominantly unidirectional rupture pulses on this strand and fault system [*BenZion et al.*, 2012].

The depth of the most recent episode of deformation varies along the strike of the NIRC fault system, which poses interesting questions regarding the extent and timing of past earthquakes and their deformation characteristics. In the north, on the Dana Point and Camp Pendleton segments, the deformation reaches very near or at the seafloor, but the transgressive surface is not displaced along great lengths of the southern extent of these parallel strands (near the San Onofre Nuclear Generating Station (SONGS)). In contrast, along the northern half, the NIRC fault zone deforms the transgressive surface on many lines from Newport Beach to approximately 12 km south of Dana Point. The upper limit of visible deformation is deepest in the central region of the area of study, Carlsbad Canyon segment, and southern portion of the Camp Pendleton segment (i.e., offshore San Onofre). A potential hypothesis is that this section of the fault zone has been inactive for a much longer period of time than the northern and southern regions and thus could be a moribund segment that highlights a dearth of throughgoing ruptures along it. In this case, the slip could be partitioning onto another adjacent fault such as the Carlsbad trend (Figure 6). Given the lack of recent deformation along this segment, the lack of activity may have existed for potentially 100 ka or more. Another hypothesis to explain this observation is that the middle section may not have experienced surface rupture in past events.

This study's interpretation of the offshore NIRC fault zone agrees reasonably well and builds on previous studies and characterizations [*Fischer and Mills*, 1991; *Treiman and Lundberg*, 1999; *Hogarth et al*., 2007; *Ryan et al*., 2009]. For example, *Hogarth et al.* [2007] observes a left step in the fault just after it moves offshore north of Mount Soledad. *Ryan et al*. [2009] describes the fault strike on various segments from La Jolla/Mount Soledad to Newport Beach, as well as the recency of deformation on the fault. *Ryan et al.* [2009] interpret three main segment boundaries in the NIRC fault zone: Del Mar/Torrey Pines (as noted by *Hogarth et al.* [2007]), Carlsbad Canyon (defined by a change in strike), and San Onofre.

One of the most detailed and oldest mappings of the fault zone (and the main contribution to the USGS NIRC mapping) is the study of *Fischer and Mills* [1991]. They characterize the offshore portion of the NIRC fault zone as being a continuous fault zone with two main stepovers offshore. Their mapping includes the Del Mar segment, running from La Jolla (Mount Soledad) to Carlsbad; the Oceanside segment, running from Encinitas to Las Pulgas Canyon or San Onofre; and the Dana Point segment, running from Las Pulgas Canyon to Newport Beach. Their offshore stepovers include the Carlsbad-Encinitas "overstep," where their Del Mar and Oceanside segments overlap, and the San Onofre left step, between the Oceanside and Dana Point segments. They note a few asperities, not described as stepovers, such as a 40° asperity by La Jolla (as the fault steps offshore), a 20° asperity by Carlsbad, and a 4° asperity by SONGS.

Similar to *Fischer and Mills* [1991], this study has the Northern strand (Dana Point segment in *Fischer and Mills* [1991]) as trending from Newport Beach to Las Pulgas Canyon, where it is separated from the next strand (here called the Carlsbad Canyon strand or the Oceanside segment in *Fischer and Mills* [1991]) by a left step, the San Onofre stepover. In this northern section of the NIRC fault zone, it differs from *Fischer and Mills* [1991]; in that, it separates the Northern strand or segment into two separate splays.

Our investigation differs further from previous studies in the southern section of the NIRC fault zone, south of San Onofre. Here the NIRC fault zone is mapped as three strands or segments until La Jolla, with two stepovers. This study's central stepover, the Carlsbad Canyon step, appears to be where *Fischer and Mills* [1991] describe a 20° asperity. The Carlsbad-Encinitas overstep from *Fischer and Mills* [1991] is where this study maps the NIRC fault zone as a continuous Carlsbad Canyon strand, diverging from the San Onofre trend. Finally, this study has separated the Del Mar segment into two strands—the La Jolla strand and the Torrey Pines strand, separated by the Torrey Pines stepover (the widest stepover in this study).

Fischer and Mills [1991] describe the age of deformation on the NIRC fault zone as being fairly young in the northern section, with Holocene faulting. In the central section of the fault zone, on the Oceanside segment by Carlsbad, they note older (or deeper) deformation, late Pleistocene/early Holocene. Moving south on the Del Mar segment they note the deformation to be very young, with very little to no Holocene sediment overlying the fault, describing the age of deformation to be early Holocene or younger. Although the segments and stepovers differ along the fault zone between this study and *Fischer and Mills* [1991], the depth (and thereby) age of deformation interpretations are consistent, describing young deformation in the north, with some undeformed sediments overlying the fault zone; older (or deeper) deformation in the central segment, by Carlsbad; and very recent, surface deformation in the southern section.

One question that arises from the results of this study relates to strain partitioning between strands. As noted, it appears that north of Las Pulgas Road near San Onofre, deformation associated with the NIRC fault zone is distributed along many strands. Additionally, the slip rate at Newport Beach, approximately ~0.5 mm/yr [*Freeman et al*., 1992; *Grant et al*., 1997], is lower than NIRC slip rate in the south by La Jolla, where it is estimated to be 1–2 mm/yr [*Lindvall and Rockwell*, 1995; *Rockwell*, 2010]. It is noted by some [*Freeman et al*., 1992] that the onshore northern region of the NIRC fault zone is characterized by splays and en echelon faulting and that this may inhibit geologic observations from capturing the full slip rate of the fault and complicate identification of active traces. This study could perhaps be observing the same phenomenon offshore. Although geodetic data are absent offshore, high-resolution 3-D geophysical surveys that identify and measure piercing point offsets combined with coring efforts could help to understand the distribution of slip through the system.

5.2. Coulomb Stress Models

An important consideration for seismic hazard analysis is whether fault segments in close proximity to each other can link up during coseismic rupture and generate a larger event. *Wesnousky* [2006] studied patterns of

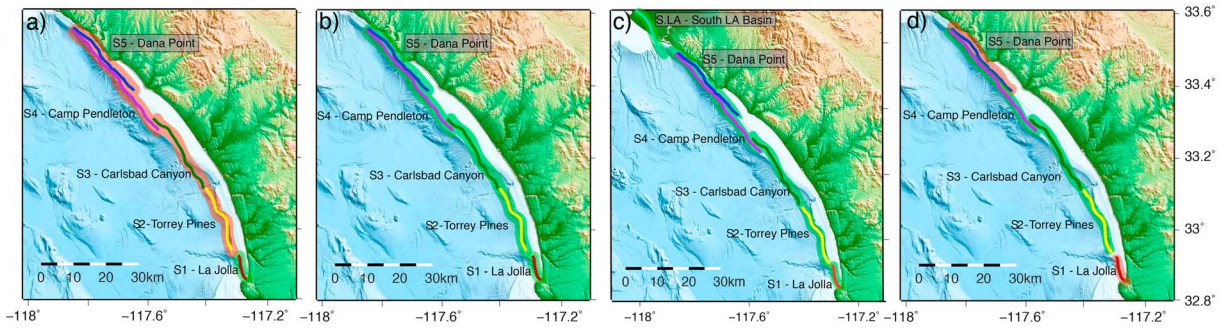

Figure 16. Examples of rupture scenarios motivated by modeling the static Coulomb stress change. Green indicates rupture on a strand, and red indicates no rupture on the strand. The strand colors are the same as in Figures 8 and 9. (a) Scenario I (Figure 13), in which rupture is initiated on the La Jolla strand. It is unlikely that the other strands will rupture. (b) Scenario II (Figure 14)—this scenario depicts all strands rupturing if the event initiates on the Carlsbad Canyon strand. Ruptures on the two splays of the Northern strand share the slip. (c) Scenario IIb—same as Scenario II, including rupture of the onshore South Los Angeles Basin segment. (d) Scenario III corresponds to Figure 15, for which all strands rupture except the Dana Point and La Jolla strands, if the event is initiated on the Camp Pendleton splay of the Northern strand.

throughgoing rupture at strike-slip fault steps, from a compilation of historical earthquakes, to determine the likelihood that an event could rupture through a stepover of given width and tectonic regime. Regardless of tectonic regime (transpressive or transtensional), events were significantly more likely to rupture through a stepover boundary with a width of 3 km or less [*Wesnousky*, 2006]. The stepovers identified in this study are all 2 km in width or less. Accordingly, the geometry of the NIRC fault zone does not preclude that a rupture will continue through all three stepovers, in which case it is possible that all of the offshore segments of the NIRC fault zone may rupture in a single event.

Based on these empirical relationships, the likelihood of an end-to-end rupture is >30–40%; rupture continuation is possible because all stepovers are <3 km in width [*Wesnousky*, 2006]. Models of static Coulomb stress change are a simple way of distinguishing more likely from less likely scenarios rather than ruling scenarios in or out. The numerical modeling results of static stress change presented here suggest that when considering only the static stress change at the computed depth of 6 km, the La Jolla/Torrey Pines stepover could possibly act as an inhibitor to throughgoing rupture because of the average dip change across the strand. This is only one consideration, however, in the likelihood of throughgoing rupture, as the effects of dynamic stress could be significantly greater and present a much larger contribution to triggering the next strand to rupture. As these are hypothetical scenarios for the NIRC, it is difficult to determine this likelihood based on just the static models; however, it should be noted that there have been studies of past events, investigating the amount of static stress change from one strand to another, given the known rupture properties of an event. One such study was conducted for the North Anatolian Fault in the August 1999 Izmit earthquake to understand triggering of adjacent segments in a stepover [*Lettis et al.*, 2002], and the modeling validated the observations. Their results for the Izmit earthquake confirmed the hypothesis posed by *Wesnousky* [2006] and demonstrated that adjacent fault segments in the Izmit earthquake could be triggered from only 1 MPa of modeled increase in Coulomb stress change.

Table 2. Computed Magnitudes for Each Scenario Rupture Presented Here[a]

Rupture Scenario	Strands	Total Rupture Length	Wells-Coppersmith	Slip: 0.5 m, μ: 20 GPa	Slip: 0.5 m, μ: 45 GPa	Slip: 2 m, μ: 20 GPa	Slip: 2 m, μ: 45 GPa
Scenario I (La Jolla strand—Figure 11)	S1	8 km	*M* 5.7 ± 0.11	*M* 6.0	*M* 6.2	*M* 6.4	*M* 6.6
Scenario II (All strands—Figure 12)	S1, S2, S3, S4, S5 (1/2 slip on S4 and S5)	125 km	*M* 7.3 ± 0.16	*M* 6.7	*M* 6.9	*M* 7.1	*M* 7.3
Scenario IIb (4 strands + Northern onshore segment)	S1, S2, S3, S4, S5, S. LA (1/2 slip on S4 and S5)	158 km	*M* 7.3 ± 0.16	*M* 6.7	*M* 7.0	*M* 7.1	*M* 7.4
Scenario III (4 strands—Figure 13)	S2, S3, S4	89 km	*M* 7.2 ± 0.16	*M* 6.6	*M* 6.9	*M* 7.0	*M* 7.3

[a]S1: La Jolla strand; S2: Torrey Pines strand; S3: Carlsbad Canyon strand; S4: Northern strand, Camp Pendleton splay; S5: Northern strand, Dana Point splay; S. LA: South Los Angeles basin segment, from *Treiman and Lundberg* [1999].

Rupture models that incorporate dynamic stress show a much greater effect on the likelihood of throughgoing rupture, as the pattern and intensity of increased Coulomb stress are greater [*Antonioli et al.*, 2004; *Kilb et al.*, 2002]. Previous studies investigating the effects of dynamic stress on the likelihood of throughgoing rupture through stepovers have found similar results to the empirical studies, showing that rupture is more likely to continue through stepovers with widths less than 5 km [*Harris and Day*, 1993]. They also offer insight into additional parameters besides stepover width that can influence the outcome of rupture propagation, such as supershear rupture on the segment with rupture initiation, smaller or intermediate fault segments within stepovers, complex fault geometries, higher stress drops, or bimaterial fault effects [*Harris and Day*, 1993; *Oglesby*, 2008; *Zaliapin and Ben-Zion*, 2011; *Lozos et al.*, 2012, 2015]. Although models of static stress change cannot include these effects, the results of the *Lettis et al.* [2002] study validate that models of static stress change can contribute valuable information in determining the possibility of throughgoing rupture on adjacent strands. At the least, static stress models can serve as a lower bound on the likelihood of rupture propagation, as the dynamic stresses during an earthquake would likely be much greater, and affect a wider spatial area [*Kilb et al.*, 2002; *Antonioli et al.*, 2004].

On this note, this study only considered static stress models with 2 m of coseismic displacement, as it intended to investigate a "high-slip scenario" to support and corroborate if rupture is possible along all strands as predicted by empirical studies of *Wesnousky* [2006]. It appears from the models of static stress change with 2 m of coseismic slip, static stress changes could allow for an end-to-end rupture of the NIRC offshore fault segments. It should be noted that future studies seeking to improve constraints of seismic hazard from this fault should consider models of dynamic stress during rupture to fully capture these effects. Furthermore, the mapping results of this study can provide important site-specific geometrical constraints for models of dynamic rupture, a consideration shown to provide important insights into the behavior of the system [*Lozos et al.*, 2015].

The models of static stress change discussed in section 4.2 motivate four potential rupture scenarios along the NIRC fault. Each scenario is represented by a four-plot figure, in which each plot shows the static stress change from one strand to the next, assuming that the ruptures were to move north or southward. In Scenario I, represented by four plots in Figure 13, rupture on the dipping La Jolla source fault (63°SW) decreases the Coulomb stress along the Torrey Pines terminus and strand to the north of the Torrey Pines stepover (Figure 13a). Therefore, it is possible that rupture on the La Jolla strand may not promote throughgoing rupture on to the Torrey Pines strand, in effect limiting the potential magnitude of the earthquake. If ruptures were to continue north onto the Torrey Pines strand, the static Coulomb stress modeling suggests that it increases the likelihood that all NIRC strands would rupture yielding a larger-magnitude earthquake (Figures 13b–13d).

The remaining scenarios (II, IIb—rupture from the central Carlsbad Canyon strand, and III—rupture from the Camp Pendleton strand) in this study propose that the possibility still exists for all or multiple offshore strands to rupture in one event (Figures 14 and 15). In the worst-case scenario, Scenarios II and IIb (illustrated through four plots in Figure 14), rupture on the Carlsbad Canyon significantly increases stress on almost all other segments moving northward and southward from the Carlsbad Canyon strand, potentially allowing for rupture on all of the NIRC offshore strands. Although the La Jolla strand experiences only a moderate amount of stress increase, this scenario considers the possibility that it ruptures. The final scenario (III) presented here considers rupture on the Camp Pendleton splay of the Northern strand. In this scenario, stress is increased by a moderate to significant amount on all segments, except for the Dana Point splay, which lies in its stress shadow. Scenario III would account for rupture on three of the four strands, as it assumes the possibility that the La Jolla strand does not rupture, unlike Scenario II (Figure 15).

Figure 16 illustrates the strands assumed to rupture for each scenario. Green shading implies that the strand ruptures, and red shading implies that it does not. Figure 16a corresponds to Scenario I (Figure 13), with rupture only on the La Jolla strand. Figure 16b corresponds to Scenario II (Figure 14) in which all strands rupture, with initial rupture on the Carlsbad Canyon strand. Figure 16c corresponds to Scenario IIb, which includes the possibility of Scenario II rupture continuing onto the onshore South Los Angeles Basin segment [*Treiman and Lundberg*, 1999] but not onto the North Los Angeles Basin segment. Finally, Figure 16d illustrates the third scenario, for rupture on the Camp Pendleton splay of the Northern strand, in which only two additional strands also rupture.

The data and models presented here suggest that it is possible to have an end-to-end rupture on the NIRC fault zone. The depth of the most recent episode of deformation on the Carlsbad Canyon strand is much

deeper than other strands, suggesting that perhaps it has been longer since this strand ruptured or that it had not experienced surface rupture. According to this observation, it could be considered that perhaps this strand is partitioning its strain onto another strand and as such is less likely to experience a rupture; however, this is not our preferred interpretation.

5.3. Scenario Magnitudes

Table 2 summarizes the potential rupture magnitudes for these scenarios. We use two methods of magnitude computation to provide both results based on empirical observations, as well as hypothetical situations of rupture. The first method of computation, based on empirical relationships, employed the Wells-Coppersmith 1994 regression parameters from their Table 2A [*Wells and Coppersmith*, 1994], relating strike-slip subsurface rupture to earthquake magnitude. Subsurface rupture length was considered as opposed to surface rupture length for two reasons. The first is that the seismic data presented in this study constrain deformation at depth, and therefore, this parameter was presumed to be a more appropriate measure of rupture length for this study. Second, *Wells and Coppersmith* [1994] mention that they found subsurface rupture length to be a more appropriate measure of magnitude because events often cause deformation at depth for a longer segment of fault than at the surface, and ground rupture is not always observed.

The second method of magnitude computation, serving as a hypothetical case of rupture properties, used seismic moment. Here the fault area was computed with the total rupture length for each scenario (Table 2) and an approximate depth for the downdip extent of rupture. In this region, the depth of microseismicity (assumed to be the brittle-ductile transition) ranges from approximately 10 to 15 km [*Astiz and Shearer*, 2000], so the depth used for the calculation of fault area was 13 km. Two values of shear modulus were used as end-members: 20 GPa and 45 GPa. These values were derived from the *P* and *S* wave velocities of a 1-D profile on the shelf near Oceanside, from the Southern California Earthquake Center Community Velocity Model–Harvard (SCEC CVM-H) [*Shaw et al*., 2015]. Two values of slip were also used as examples of a lower and upper bound: 0.5 m coseismic slip and 2 m coseismic slip. A conservative upper bound for this model is based on coseismic slip observed in a paleoseismic trench by *Lindvall and Rockwell* [1995] and *Rockwell* [2010], which stated that one location may have experienced up to 3 m of coseismic slip in one event.

The lowest potential magnitudes computed, *M* 5.7–6.6, were derived from Scenario I, with slip solely on the La Jolla strand, from Mount Soledad. Scenario III provides an intermediate case, for which magnitudes could be expected at *M* 6.6 to 7.3. The largest potential event stems from Scenario II, or slip on all offshore strands—at *M* 6.7–7.3, which increases to 7.4 if the northern onshore segment ruptures also (IIb). Magnitudes computed for Scenarios II and IIb assume that the slip is partitioned on the northern two splays (Camp Pendleton and Dana Point splays), as they are subparallel and in close proximity for the majority of their strike, suggesting that they may connect at depth. Accurate fault representations are a crucial component of seismic hazard models as fault geometry constrains potential rupture sequences and maximum event magnitudes. Studies such as this one are key in improving the geometry and length of rupture as input into models like UCERF3 [*Field et al*., 2014], as they constrain the fault architecture, segment length, linkage of segments, and propagation of rupture across stepovers or segment boundaries. Although many uncertainties remain, imaging fault architecture and Coulomb stress modeling can serve as a basis and guide to focus the direction of future observational and modeling studies on this fault zone, in particular modeling of the dynamic stresses during rupture to capture effects not shown by static stress models.

6. Conclusions

Through the use of nested active-source seismic reflection data, this study identified four main strands of the offshore NIRC fault zone (with the northern strand consisting of two parallel splays) and three stepovers of approximate widths of 2 km or less. It improves the characterization of offshore fault geometry and provides rupture scenarios based on triggering across these fault stepovers due to static stress changes. Through these investigations, it has been determined that changes in fault dip and strike at the Torrey Pines stepover could possibly limit the rupture extent of earthquakes along the NIRC fault zone, although dynamic stress modeling should be conducted to further investigate this prediction. Finally, it has revealed that based on these new

mappings and insights, an end-to-end rupture of the offshore portion of the NIRC fault zone could, depending on rupture characteristics, produce a *M* 7.3 earthquake or a *M* 7.4 event if a northern onshore segment is included. If rupture were to occur on the southern onshore portion of the fault as well, the magnitude would be even greater. This work highlights the contribution of offshore faults toward the combined seismic risk for Southern California. Further study is warranted to improve the current understanding of hazard and potential ground shaking posed to urban coastal areas from Tijuana to Los Angeles from the NIRC fault zone and other faults in the ICB.

Acknowledgments

This work was funded by Southern California Edison. The Chevron 1979 and USGS 2006 data were downloaded from the U.S. Geological Survey Coastal and Marine Geoscience Data System (cmgds.marine.usgs.gov). The reprocessed data are archived in the Academic Seismic Portal at the University of Texas at Austin Institute for Geophysics (UTIG) [*Driscoll et al*., 2013]. The CHIRP, high-resolution, and 2013 MCS data were collected and processed in-house and have been uploaded to the Lamont-Doherty Earth Observatory NSF database as well as UTIG's Academic Seismic Portal repository. The data will be open source in 2017. The multibeam data were processed using the Caris HIPS and SIPS software (www.caris.com/products/hips-sips), and the CHIRP data were processed using SIOSEIS (sioseis.ucsd.edu) and Seismic Unix (www.cwp.mines.edu/cwpcodes). Reprocessing of the 1979 Chevron data was performed by Geotrace (www.geotrace.com), and reprocessing of the 2006 USGS data was conducted at SIO/UC San Diego using MATLAB. Map figures were created using Generic Mapping Tools, available at http://gmt.soest.hawaii.edu/). Special thanks to the crew of the R/V *New Horizon* and the R/V *Melville* as their efforts allow scientists access to the sea. The authors also would like to thank Debi Kilb for her insight and comments on the work, as well as an anonymous reviewer and Joann Stock for their salient and helpful reviews that improved the quality of the manuscript.

References

Antonioli, A., M. E. Belardinelli, and M. Cocco (2004), Modelling dynamic stress changes caused by an extended rupture in an elastic stratified half-space, *Geophys. J. Int.*, *157*(1), 229–244, doi:10.1111/j.1365-246X.2004.02170.x.

Astiz, L., and P. M. Shearer (2000), Earthquake locations in the Inner Continental Borderland, offshore Southern California, *Bull. Seismol. Soc. Am.*, *90*(2), 425–449, doi:10.1785/0119990022.

Bennett, R. A., W. Rodi, and R. E. Reilinger (1996), Global positioning system constraints on fault slip rates in Southern California and northern Baja, Mexico, *J. Geophys. Res.*, *101*(B10), 21,943–21,960, doi:10.1029/96JB02488.

BenZion, Y., T. Rockwell, Z. Shi, and S. Xu (2012), Reversedpolarity secondary deformation structures near fault stepovers, *J. Appl. Mech.*, *79*, 031,025, doi:10.1115/1.4006154.

Berkhout, A. J., and D. J. Verschuur (1997), Estimation of multiple scattering by iterative inversion, Part I: Theoretical considerations, *Geophysics*, *62*(5), 1586–1595, doi:10.1190/1.1444261.

Dartnell, P., N. W. Driscoll, D. Brothers, J. E. Conrad, J. Kluesner, G. M. Kent, and B. Andrews (2015), Colored shaded-relief bathymetry, acoustic backscatter, and selected perspective views of the Inner Continental Borderland, Southern California, U.S. Geological Survey Scientific Investigations Map 3324, 3 sheets, Southern California, U.S. 10.3133/sim3324.

Driscoll, N., G. Kent, and J. Bormann (2013), Processed multi-channel seismic data (stacks and migrations) offshore California acquired during the R/V *New Horizon* expedition NH1320 (2013) using a sparker source: Academic Seismic Portal at UTIG, Marine Geoscience Data System, doi:10.1594/IEDA/500041.

Field, E. H., et al. (2014), Uniform California Earthquake Rupture Forecast, version 3 (UCERF3)—The time-independent model, *Bull. Seismol. Soc. Am.*, *104*(3), 1122–1180, doi:10.1785/0120130164.

Fischer, P. J., and G. I. Mills (1991), The offshore Newport-Inglewood Rose Canyon fault zone, California: Structure, segmentation, and tectonics, in *Environmental Perils San Diego Region: San Diego Region: San Diego Association of Geologists*, edited by P. L. Abbott and W. J. Elliot, pp. 17–36, San Diego, Calif.

Freeman, S. T., E. G. Heath, and P. D. Guptill (1992), in *Seismic Hazard Assessment, Newport-Inglewood Fault Zone*, vol. 4, edited by B. W. Pipkin and R. J. Proctor, pp. 211–231, Assoc. of Eng. Geol., Star Publishing Company, Belmont, Calif., doi:10.1029/95JB02627/pdf.

Grant, L. B., and P. M. Shearer (2004), Activity of the offshore Newport-Inglewood Rose Canyon fault zone, coastal Southern California, from relocated microseismicity, *Bull. Seismol. Soc. Am.*, *94*(2), 747–752, doi:10.1785/0120030149.

Grant, L. B., and T. K. Rockwell (2002), A northward-propagating earthquake sequence in coastal Southern California?, *Seismol. Res. Lett.*, *73*(4), 461–469, doi:10.1785/gssrl.73.4.461.

Grant, L. B., J. T. Waggoner, T. K. Rockwell, and C. von Stein (1997), Paleoseismicity of the north branch of the Newport-Inglewood fault zone in Huntington Beach, California, from cone penetrometer test data, *Bull. Seismol. Soc. Am.*, *87*(2), 277–293.

Harris, R. A., and S. M. Day (1993), Dynamics of fault interaction: Parallel strike-slip faults, *J. Geophys. Res.*, *98*(B3), 4461–4472, doi:10.1029/92JB02272.

Hauksson, E., and S. Gross (1991), Source parameters of the 1933 Long Beach earthquake, *Bull. Seismol. Soc. Am.*, *81*(1), 81–98.

Hogarth, L. J., J. Babcock, N. W. Driscoll, N. Le Dantec, J. K. Haas, D. L. Inman, and P. M. Masters (2007), Long-term tectonic control on Holocene shelf sedimentation offshore La Jolla, California, *Geology*, *35*(3), 275–278, doi:10.1130/G23234A.1.

Holmes, J., J. Bormann, N. W. Driscoll, G. M. Kent, A. J. Harding, and S. G. Wesnousky (2014), New high-resolution 3D seismic imagery of deformation and fault architecture along Newport-Inglewood/Rose Canyon fault in the Inner California Borderlands, Abstract OS33A-1035 presented at the 2014 AGU Fall Meeting, San Francisco, Calif., 15–19 Dec.

Kilb, D., J. Gomberg, and P. Bodin (2002), Aftershock triggering by complete Coulomb stress changes, *J. Geophys. Res.*, *107*(B4), 2060, doi:10.1029/2001JB000202.

King, G. C. P., and J. F. Nabelek (1985), Role of fault bends in the initiation and termination of earthquake rupture, *Science*, *228*, 984–987.

Klotsko, S., N. W. Driscoll, G. Kent, and D. Brothers (2015), Continental shelf morphology and stratigraphy offshore San Onofre, California: The interplay between rates of eustatic change and sediment supply, *Mar. Geol.*, *369*, 116–126.

Lettis, W., et al. (2002), Influence of releasing stepovers on surface fault rupture and fault segmentation: Examples from the 17 August 1999 İzmit earthquake on the North Anatolian Fault, Turkey, *Bull. Seismol. Soc. Am.*, *92*(1), 19–42, doi:10.1785/0120000808.

Lin, J., and R. S. Stein (2004), Stress triggering in thrust and subduction earthquakes and stress interaction between the southern San Andreas and nearby thrust and strike-slip faults, *J. Geophys. Res.*, *109*, B02303, doi:10.1029/2003JB002607.

Lindvall, S. C., and T. K. Rockwell (1995), Holocene activity of the Rose Canyon fault zone in San Diego, California, *J. Geophys. Res.*, *100*(B12), 24,121–24,132, doi:10.1029/95JB02627.

Lozos, J. C., D. D. Oglesby, J. N. Brune, and K. B. Olsen (2012), Small intermediate fault segments can either aid or hinder rupture propagation at stepovers, *Geophys. Res. Let.*, *39*, L18305, doi:10.1029/2012GL053005.

Lozos, J. C., D. D. Oglesby, J. N. Brune, and K. B. Olsen (2015), Rupture propagation and ground motion of strike-slip stepovers with intermediate fault segments, *Bull. Seismol. Soc. Am.*, *105*(1), 387–399, doi:10.1785/0120140114.

Magistrale, H. (1993), Seismicity of the Rose Canyon fault zone near San Diego, California, *Bull. Seismol. Soc. Am.*, *83*(6), 1971–1978.

Maloney, J. M., N. W. Driscoll, G. M. Kent, S. Duke, T. Freeman, and J. M. Bormann (2016), Segmentation and stepovers along strike-slip fault systems in the Inner California Borderlands: Implications for fault architecture and basin formation, in *Applied Geology in California: Association of Environmental and Engineering Geologists, Special Publication Number 26, Chapter 36*, edited by R. Anderson and H. Ferriz, pp. 655–677, Star Publishing Company, Redwood, Calif.

Oglesby, D. (2008), Rupture termination and jump on parallel offset faults, *Bull. Seismol. Soc. Am.*, *98*(1), 440–447, doi:10.1785/0120070163.

Okada, Y. (1992), Internal deformation due to shear and tensile faults in a half-space, *Bull. Seismol. Soc. Am.*, *82*(2), 1018–1040.

Riley, D. C., and J. F. Claerbout (1976), 2-D multiple reflections, *Expl. Geophys.*, *41*(4), 592–620, doi:10.1190/1.1440638.
Rockwell, T. (2010), The Rose Canyon fault zone in San Diego. Presented at the Proceeding of Fifth International Conference on Recent Advances in Geotechnical Earthquake Engineering and Soil Dynamics.
Ryan, H. F., M. R. Legg, J. E. Conrad, and R. W. Sliter (2009), Recent faulting in the Gulf of Santa Catalina: San Diego to Dana Point, *Geol. Soc. Am. Spec. Pap.*, *454*, 291–315, doi:10.1130/2009.2454(4.5).
Sargent, C., R. W. Hobbs, and D. R. Grocke (2011), Case history improving the interpretability of air-gun seismic reflection data using deterministic filters: A case history from offshore Cape Leeuwin, southwest Australia, *Expl. Geophys.*, *76*(3), B113–B125.
Shaw, J. H., et al. (2015), Unified structural representation of the Southern California crust and upper mantle, *Earth Planet. Sci. Lett.*, *415*, 1–15, doi:10.1016/j.epsl.2015.01.016.
Sibson, R. H. (1985), Stopping of earthquake ruptures at dilatational fault jogs, *Nature*, *316*, 248–251.
Toda, S., R. S. Stein, K. Richards-Dinger, and S. B. Bozkurt (2005), Forecasting the evolution of seismicity in Southern California: Animations built on earthquake stress transfer, *J. Geophys. Res.*, *110*, B05S16, doi:10.1029/2004JB003415.
Treiman, J. A., and M. Matthew Lundberg (Comps.) (1999), Fault number 127b, Newport-Inglewood-Rose Canyon fault zone, south Los Angeles Basin section, in *Quaternary Fault and Fold Database of the United States*, US Geological Survey website. [Available at http://earthquakes. usgs. gov/regional/qfaults, accessed 10 (2009): 45.]
Toda, S., R. S. Stein, V. Sevilgen, and J. Lin (2011), Coulomb 3.3 graphic-rich deformation and stress-change software for earthquake, tectonic, and volcano research and teaching-user guide, *U.S. Geol. Surv. Open File Rep., 2011*.
U.S. Geological Survey Coastal and Marine Geology Program (2006), High-resolution mini-sparker seismic data of field activity S-2-06-SC in offshore Dana Point, Orange County, CA from 09/01/2006 to 09/08/2006. *USGS*, *CMG*. Menlo Park, CA: U.S. Geological Survey.
U.S. Geological Survey and California Geological Survey (2006), Quaternary fault and fold database for the United States, accessed May 2, 2014, from USGS website. [Available at http://earthquake.usgs.gov/hazards/qfaults/.]
Verschuur, D. J., and A. J. Berkhout (1997), Estimation of multiple scattering by iterative inversion, Part II: Practical aspects and examples, *Geophysics*, *62*(5), 1596–1611.
Wells, D. L., and K. J. Coppersmith (1994), New empirical relationships among magnitude, rupture length, rupture width, rupture area, and surface displacement, *Bull. Seismol. Soc. Am.*, *84*(4), 974–1002.
Wesnousky, S. G. (2006), Predicting the endpoints of earthquake ruptures, *Nature*, *444*(7117), 358–360, doi:10.1038/nature05275.
Wood, H. O. (1933), Preliminary report on the Long Beach earthquake, *Bull. Seismol. Soc. Am.*, *23*(2), 43–56.
Yilmaz, O. (2001), *Seismic Data Analysis*, vol. 1, Society of Exploration Geophysicists, Tulsa, Okla.
Zaliapin, I., and Y. Ben-Zion (2011), Asymmetric distribution of aftershocks on large faults in California, *Geophys. J. Int.*, *185*, 1288–1304, doi:10.1111/j.1365-246X.2011.04995.x.